Med Biol Eng Comput
DOI 10.1007/s11517-010-0648-4

ORIGINAL ARTICLE

Automatic video detection of body movement during sleep based on optical flow in pediatric patients with epilepsy

Kris Cuppens · Lieven Lagae · Berten Ceulemans · Sabine Van Huffel · Bart Vanrumste

Received: 7 August 2009 / Accepted: 2 June 2010
© International Federation for Medical and Biological Engineering 2010

Abstract The aim of our work is to investigate whether the optical flow algorithm applied to video recordings can be used to detect movement during sleep in pediatric patients with epilepsy. The optical flow algorithm allocates intensities to pixels proportional to their involvement in movement of an object. The average of a percentage of the highest movement vectors was plotted as a function of time ($R(t)$). The used dataset contains video data acquired at the University Hospital of Leuven consisting of normal sleep movement and seizure movement. We investigated $R(t)$, to make a distinction between movement and non-movement. We used the acquisition parameters (320 × 240 at 12.5 fps), derived from a previous study (Cuppens et al., Proceedings of the 4th European congress of the international federation for medical and biological engineering (MBEC 2008), ECIFBME 2008, Antwerp, Belgium, IFMBE Proceedings, vol 22, pp 784–789, 2008). Two experiments were concluded, one with global thresholds of $R(t)$ in all datasets and one with a variable threshold in each dataset. The latter is obtained by inspecting a non-movement epoch and calculating the mean and standard deviations of $R(t)$ over time. The variable threshold on $R(t)$ was then obtained for each dataset by adding to the mean a fixed multiple of the standard deviation. Optimal thresholds were derived based on a three-fold cross-validation. The best result was achieved when using a variable threshold, which resulted in a sensitivity of one in all the test sets and a PPV of 1, 0.821, and 1, respectively, for the three test sets.

Keywords Epilepsy · Pediatric patients · Optical flow · Movement detection · Nocturnal recordings

K. Cuppens (✉) · B. Vanrumste
MOBILAB, K.H.Kempen, Kleinhoefstraat 4,
2440 Geel, Belgium
e-mail: kris.cuppens@khk.be; kriscuppens@gmail.com

B. Vanrumste
e-mail: bart.vanrumste@khk.be;
bart.vanrumste@esat.kuleuven.be

K. Cuppens · S. Van Huffel · B. Vanrumste
SCD/ESAT, KULeuven, Kasteelpark Arenberg 10,
3001 Heverlee, Belgium
e-mail: sabine.vanhuffel@esat.kuleuven.be

L. Lagae
Kindergeneeskunde, UZLeuven, Herestraat 49,
3000 Leuven, Belgium
e-mail: lieven.lagae@uz.kuleuven.ac.be

B. Ceulemans
Kinderneurologie, UZA, Wilrijkstraat 10,
2650 Edegem, Belgium
e-mail: berten.ceulemans@uza.be

Published online: 24 June 2010

1 Introduction

The golden standard for the detection of epileptic seizures is video-electroencephalogram monitoring. This method, however, is patient-demanding as the attached electrodes are uncomfortable to wear for long-time monitoring. Moreover, it is labor-intensive for the technical staff as it takes 20–40 min to glue all the electrodes on the scalp. Furthermore a low impedance between the electrode and the scalp is required to have a good acquisition of the EEG. Hence, multiple weeks of home monitoring is not feasible.

During the recent years, numerous researchers have come up with different solutions for the monitoring of patients, based on different types of sensors, e.g., Schepers et al. [18] used three-dimensional accelerometers and three-dimensional gyroscopes in combination with three-

dimensional magnetometers to track human motion. Suzuki et al. [20] monitor human respiration and heart beat in a non-contacting way by means of microwave radars. But also video is used for monitoring humans, e.g., Bonroy et al. [1] monitor the visual expression of humans using a camera system for pain assessment. This automatic vision-based monitoring can also be a solution for monitoring of epileptic patients.

Motion detection or segmentation in video can be done in different ways. Some of the most used methods are *temporal differencing, background modeling and subtraction,* and *optical flow* [8, 13, 22]. Other methods can be based on *point trajectories* or *spatio-temporal filter responses* [21]. Wang et al. [22] mentioned in their survey some techniques which could be found in literature such as an extended expectation–maximization algorithm, a mixture of Gaussians classification model and a morphological algorithm for scene change detection. Our approach uses optical flow as the calculated flow vectors give an indication of the strength of the motion which is used in our algorithm.

The most common implementations of the optical flow algorithm are the Horn–Schunk method [7] which makes use of a smoothness constraint to solve the aperture problem and the Lucas–Kanade [15] method which assumes that the flow in small sections of pixels is the same.

Although movement detection is most studied in surveillance, some steps are already taken for the detection of epileptic seizures in adults [14] and neonates [10]. Liu et al. [14] detected changes between video frames in a certain sequence of video data from epileptic seizures. This is comparable with the detection of movement. They developed an accurate and robust algorithm for change detection. To visualize this, a *Change Detection Map* (CDM) was constructed which shows the detected motion in the subsequent images. The algorithm was tested on MATLAB generated images as well as on real data of epileptic patients, however, no information about sensitivity and specificity of their method are given in their paper. The CDM computed in this algorithm holds no information about the intensity of the movement. In contrast, the optical flow gives this information in our approach.

Karayiannis et al. [10] shows that the detection of convulsions (epileptic seizures with a motor component) in neonates is possible with a camera system. They investigate features to detect myoclonic and focal clonic seizures. Their algorithm shows promising results for these types of seizures. Karayiannis' work differs from our work in the fact that we monitor children up to the age of 18 whereas his work monitors neonates who may have a different manifestation of seizures. Moreover, his study monitors the patients in a setting where the extremities are well visible to the camera, while in our datasets, the patients are most of the time covered with a blanket.

Another novel approach to reveal epileptic seizures with motor activity is the detection by means of accelerometers. Nijsen et al. [16] has developed a detection algorithm to discriminate between data with and without subtle nocturnal motor activity. Five accelerometers were attached to the body, two to the ankles, two to the wrists, and one to the chest. The algorithm detected all the motor events, and 43–89% of the detections was correct. Jallon et al. [9] and Cuppens et al. [6] also studied the detection of epileptic seizures with accelerometers and Conradsen et al. [4] used a multi-modal approach. In our approach, we detect the movement contactless, which is more comfortable for the patient.

The aim of this paper is the detection of movement based on video data, using the Horn–Schunck optical flow method. More specifically, we determine the optimal thresholds to distinguish movement from non-movement epochs, which we tested using a three-fold cross-validation.

The remainder of this paper is organized as follows: in Sect. 2 the acquisition of the data, the methods used in the motion detection algorithm, and the measures used to validate the algorithm are described. Section 3 shows the results of the detection algorithm and in this section ideal thresholds are determined to discriminate between movement and non-movement. Section 4 covers the discussion ending in a concluding statement.

2 Method

2.1 Video acquisition

We obtained the video data from the University Hospital Leuven (Belgium), using a database of epileptic seizures from the Department of Child Neurology. The video sequences were compressed with an MPEG-1 compression before they were stored. The resolution of the used video data was 320 × 240 with a frame rate of 25 fps. The video data was acquired by BrainRT-software (http://www.brainrt.com/). The data was labeled, i.e., the starting and ending points in time of the movement epochs (including epileptic seizures) were marked by an expert. Each sequence (epoch) contains a movement event. The length of the events ranges from 1 to 304 s. An overview of the video sequences is given in Table 1. The infrared camera was placed according to the sketch in Fig. 1. The video was zoomed in on the patient in a way that the head, the arms, and the torso was visible in videos 1, 3, 4, 5, 7, 8, and 11. In the other videos the whole patient was visible.

The dataset consisted of a 1 h 48 min and 44 s recording with 73 movement events from which 11 were convulsions.

Table 1 Overview obtained video sequences containing movement

Sequence	Length	Movements	Epileptic movements	Patient	Training set	Test set
1	15 min	9	1	a	1, 2	3
2	15 min	17	0	b	2, 3	1
3	15 min	7	0	c	1, 2	3
4	15 min	4	0	c	1, 3	2
5	15 min	3	0	c	2, 3	1
6	30 min	16	0	d	1, 3	2
7	30 s	4	3	e	1, 3	2
8	34 s	2	1	f	2, 3	1
9	1 min 55 s	7	4	g	1, 2	3
10	26 s	1	1	h	1, 3	2
11	19 s	3	1	f	2, 3	1
Total	1 h 48 min 44 s	73	11			

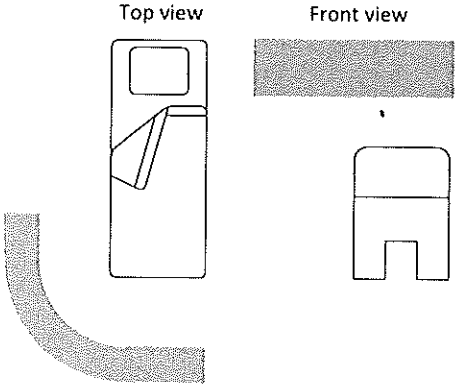


Fig. 1 A sketch of the camera positions in the different video sequences. The marked areas indicate the place where the camera is placed

This dataset is a sequence of 11 recordings from eight patients between the age of 9 months and 16 years.

The inclusion criteria for the sequences to be a part of the dataset are the following:

- The recorded patients should be maximum 18 years of age.
- The recordings are taken in a nocturnal setting, a blanket is allowed.
- The video data is recorded with an infrared camera, hence grayscale images.
- The sequences should contain at least one movement epoch, which does not necessarily have to be of epileptic nature.

2.2 Optical flow algorithm

The optical flow algorithm calculates the velocity vectors in each pixel in every frame of a video sequence, based on the change in the pixel intensities. It gives a two-dimensional representation of three-dimensional motion [11]. For the calculation of the velocity vectors, the assumption is made that the intensity of a pixel from the image of an object does not change as the pixel moves from frame to frame, this is the so called *brightness constraint*. This means that we assume that the brightness of a pixel does not change as it is tracked from frame to frame [2, 12].

The image brightness at point (x, y) in the image at time t can be denoted as $I(x, y, t)$. The brightness at a certain point is considered constant in time as given in the brightness constraint. If the point moves dx in the x-direction and dy in the y-direction in a time dt, the brightness of the point stays constant [7], by which

$$I(x, y, t) = I(x + dx, y + dy, t + dt), \tag{1}$$

The right-hand side can be expressed as a Taylor series [19]:

$$I(x + dx, y + dy, t + dt) = I(x, y, t) + I_x dx + I_y dy + I_t dt + O(\delta^2). \tag{2}$$

$O(\delta^2)$ represents the second and higher order terms, and I_x, I_y, and I_t are the partial derivates of I. If dx, dy and dt are very small, the higher order terms in Eq. 2 vanish and this equation can be rewritten as

$$I_x \frac{dx}{dt} + I_y \frac{dy}{dt} + I_t = 0, \tag{3}$$

where $u = \frac{dx}{dt}$ and $v = \frac{dy}{dt}$ are the velocities in the horizontal and vertical direction, respectively. These values represent the movement we want to calculate. A further elaboration can be found in Horn and Schunck [7].

2.3 Detection algorithm

The goal of the detection algorithm is to distinguish epochs with movement from epochs without movement. The

optical flow algorithm calculates a vector field with a motion vector in each pixel, as shown in Fig. 2b, considering Fig. 2a as one frame of the video sequence of a child that moves its left arm. For the further calculations the magnitude of each motion vector is used. This gives video images with each pixel representing the intensity of the movement (the resultant of the vector). The result of such an image is shown in Fig. 2c. As visible in this figure, several spurious pixel intensities are shown which are noise which may be introduced by the camera or by the MPEG-compression. Figure 2c is amplified with a factor of 15 to emphasize these spurious patches. To eliminate the noise, only a small amount of pixels is taken into account. The pixels with the highest movement intensity are maintained. The result of this image is shown in Fig. 2d. The number of pixels with the highest amplitude is a free parameter that needs to be determined as explained in Sect. 3.2.

The next step takes the mean of the selected vector magnitudes which results into the one-dimensional output signal (further referred to as $R(t)$ in this paper) indicating the motion in the video sequence. This signal is further examined to find the epochs with movement.

As a last step this one-dimensional signal is thresholded to discriminate between movement and non-movement.

A smaller $R(t)$ for non-movement epochs in comparison to the $R(t)$ for movement epochs facilitates the discrimination by means of thresholding between movement and non-movement epochs.

2.4 Measures

In this section, we introduce measures to analyze the performance of the algorithm under different acquisition and environmental settings, namely the *movement vs. non-movement ratio* (MNMR) and *max*$(R(t))$, and provide the tools to define the ideal threshold and the percentage of motion vectors namely the sensitivity and positive predictive value (PPV).

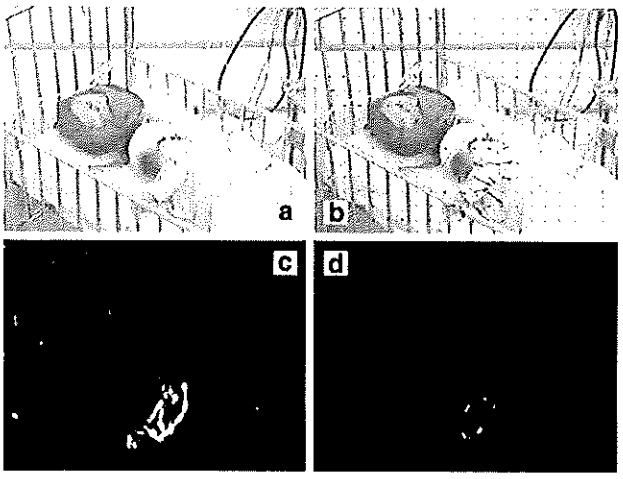


Fig. 2 Image from acquired video data (**a**) Vector field calculated by the optical flow algorithm (**b**) Optical flow image where each pixel indicates an optical flow vector's amplitude with an amplification of 15 to emphasize the spurious pixels (**c**) Image after taking 0.06% pixels with highest intensity (thus vectors with highest amplitude) (**d**)

The MNMR is defined as

$$\mathrm{MNMR} = \frac{\max(R(t))_{\text{movement}}}{\max(R(t))_{\text{non-movement}}}, \tag{4}$$

where $\max(R(t))_{\text{movement}}$ and $\max(R(t))_{\text{non-movement}}$ represent the maximum value of $R(t)$ in a movement epoch and in a non-movement epoch, respectively. It is clear, to have a good distinction between a movement and non-movement epoch, that the MNMR measure needs to be larger than 1 and preferably be as large as possible.

To get an indication of the performance of the algorithm and thus detect the best value for percentage of the vectors and the threshold, we use the sensitivity and the PPV as stated below.

$$\mathrm{Sensitivity} = \frac{\mathrm{TP}}{\mathrm{TP}+\mathrm{FN}} = \frac{\text{Correct detected epochs}}{\text{All labeled movement epochs}}, \tag{5}$$

and

$$\mathrm{PPV} = \frac{\mathrm{TP}}{\mathrm{TP}+\mathrm{FP}} = \frac{\text{Correct detected epochs}}{\text{All detected epochs}}, \tag{6}$$

where TP, FN, and FP stands for true positives, false negatives, and false positives, respectively. The *sensitivity* gives the fraction of the correct detected epochs from all labeled movements. The *PPV* gives the number of the detections which are TP. Ideally both measures are one. This movement detection algorithm is a data reduction step, and the sensitivity should be 1 because we do not want to lose significant data. Because we want as less unnecessary data as possible, the PPV should be as high as possible.

For the comparison of the events, the automatic detection and the manually labeled events are first clustered separately. If two events lie less than 4 s apart, the events are merged. The next step adds 2 s before and after each event because of the lower accuracy of the human labeler. The clustering is shown in Fig. 3b.

We compare the labeled dataset with the result of the automatic detection algorithm to calculate the TPs, FNs, and FPs. When the algorithm detects movement during a labeled event, this epoch is considered as a true positive. If we detect no movement during a labeled event, the epoch is considered as a false negative. This is visualized in Fig. 3c.

Sometimes one detected event can last for much longer than the human labeler observed. It would be preferable to detect such an event as a false positive. That is why false positives are calculated in the following way. First, the

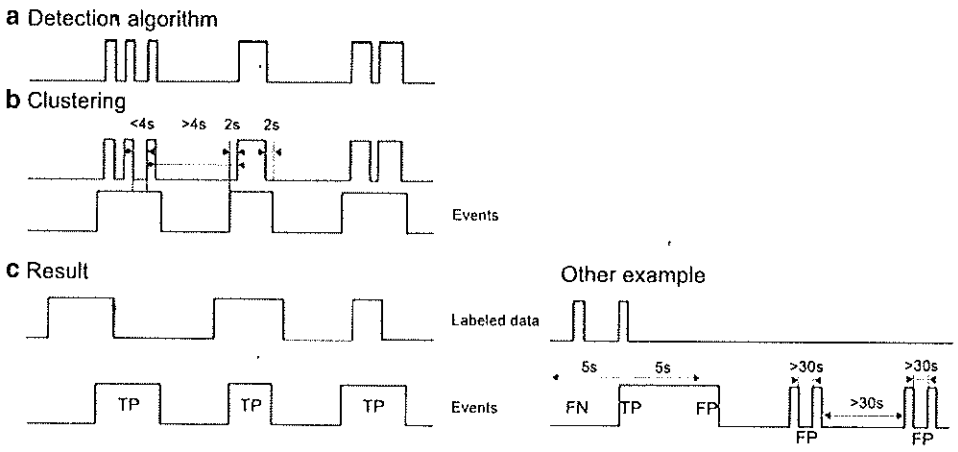


Fig. 3 Clustering of the events and classify them as TP, FP or FN. a Shows the events detected by the algorithm, b shows the clustering which is done afterwards. c Gives an overview of how the events are labeled in two examples

events labeled by the human labeler are expanded by 5 s in the beginning and at the end. Every event detected by the algorithm outside these regions is considered as a false positive.

There was one sequence with a flickering computer screen in the background. This led to an increased movement signal resulting in false positives. When the threshold is set higher in this or other similar cases, it is possible that only a few spikes cross the threshold resulting in several short false positives instead of one large false positive. This leads to a counterintuitive situation where the number of false positives increases when the threshold is set higher. To overcome this problem, false positives are clustered when they lie closer than 30 s apart.

We need to optimize two parameters. The first is the number of highest movement vectors (or fraction of highest movement vectors) that we apply to calculate $R(t)$.

The second parameter we want to optimize is the threshold we have to set on $R(t)$ to get a good distinction. We have worked out the two approaches for the threshold calculation.

2.4.1 First approach: global threshold

In the first approach, we try to find an optimal fixed threshold to distinguish between movement and non-movement for all the different video sequences. If such a threshold exists, it is not necessary to find an optimal threshold for each sequence individually, which is the most convenient solution.

2.4.2 Second approach: variable threshold

A second approach to determine the optimal threshold is to make the threshold dependent of the noise (i.e. non-movement epochs) in the sequence. Therefore a short epoch, which does not contain movement, at the start of the sequence is chosen. From this epoch the mean and standard deviation are calculated. This gives a representation of the non-movement. The threshold is determined by adding a multiple of the standard deviation to the mean of the epoch. In this way an adaptive threshold is created. We use the same multiplication factor for each sequence. This approach is tested on the same datasets as the first approach.

2.5 Cross-validation

To check the performance of the algorithm, we perform a three-fold cross-validation. For the training and test set we divide the dataset into three subsets, all containing about the same number of movement events. This partition is shown in Table 1. In each validation the training set contained two of the subsets and the test set was the remaining subset.

From each training set the most optimal parameter combination is determined, and used in the test set. The performance of each test set is then given by the sensitivity and PPV.

3 Results

3.1 Choosing acquisition parameters

In a previous study, we already investigated $R(t)$ for the number of pixels equal to 0.06% (which is close to the ideal point) for the movement in a video sequence under different environmental and acquisition parameters. In our previous study, a simulation video was recorded to represent different possible settings in the environment such as a change in illumination and the influence of acquisition settings such as the frame rate. The results of this study are presented in [5]. This section gives an overview of the most important results, using the measures to analyze the performance of the algorithm introduced in the previous section.

3.1.1 *Impact of downsampling in space*

When the video sequences are downsampled in space both $R(t)$ and the MNMR become smaller. This means that the vectors originating from a movement are decreasing more than the noise. A greater downsampling in space than 320 × 240 pixels results in a considerable lower MNMR. For this reason a resolution of 320 × 240 is used in this paper.

3.1.2 *Impact of downsampling in time*

When the signal is downsampled in time, $R(t)$ increases. This is visible in Table 2. In this table, the values for $R(t)$ during movement and non-movement and the MNMR are shown. Notice, however, that this trend is not always true when the signal is downsampled to 5 fps. When the difference between an object is too large between two consecutive frames, the optical flow calculation can be inaccurate. The increase of $R(t)$ can be explained by the fact that if an object, or body part moves at a certain speed, it has moved a longer distance between each frame if we sample at a lower frequency. Notice, however, that aliasing effects can have an influence on the correctness of the optical flow calculation. Also, due to aliasing, specific patterns in the $R(t)$ curve as shown in Fig. 4 may be lost. Such a pattern could be interesting for the detection of certain epileptic seizures, but does not play a role in the discrimination between movement and non-movement.

As we want a sufficiently high MNMR, a downsampling to 5 fps may be unwanted, as the MNMR drops substantially in the different sequences for this frame rate, also shown in Table 2.

Another observation is that the MNMR value for subtle movements is clearly smaller than bigger movements, but no clear trend can be observed regarding the MNMR when the video is downsampled in time.

Table 2 MNMR and $R(t)$ at different downsample ratios in time, with the percentage of pixels fixed at 0.06

	30 fps	15 fps	10 fps	5 fps
MNMR				
Myoclonic shock	82.0994	90.3868	103.0590	32.9629
Moving head	64.0910	30.2057	28.6357	22.8782
$R(t)$ non-movement				
Myoclonic shock	0.0350	0.0436	0.0455	0.1339
Moving head	0.0143	0.0398	0.0598	0.0540
$R(t)$ movement				
Myoclonic shock	2.8766	3.9406	4.6922	4.4143
Moving head	0.9146	1.2031	1.7111	1.2358

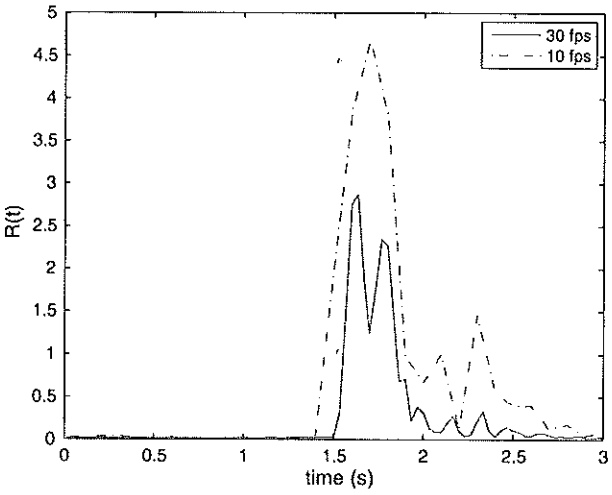


Fig. 4 Downsampling in time of myoclonic shock

As a conclusion, we can say that the temporal sample frequency should not be lower than 10 fps. In our dataset this means that we can downsample by a factor of 2 to 12.5 fps.

3.1.3 *Impact of illumination*

When the illumination is lowered, $R(t)$ stays more or less the same for movement epochs but $R(t)$ increases for the non-movement epochs.

3.2 Identifying a threshold for $R(t)$ and number of optical flow vectors

The performance of the algorithm is calculated for different values of the two parameters we want to optimize, namely the percentage of movement vectors and the threshold on $R(t)$. The percentages of movement vectors range between 0.0013 (this is one vector) and 100 (these are all the vectors), the values for the fixed threshold are between 0.005 and 1.5, the multiplication factor of the standard deviation for the variable threshold ranges between 1.5 and 30. For a proper evaluation, the dataset is split up into three subsets containing all more or less the same number of movement events. These subsets are used to perform a three-fold cross-validation. The results for both approaches are discussed below and can be found in Table 3 and Fig. 5.

3.2.1 *First approach: global threshold*

On each training set the ROC-curves are calculated as shown in Fig. 5a, e. The most optimal point on each ROC-curve has a sensitivity of one, as we do not want to miss important events, with a maximal PPV. For the first training set for the fixed threshold, this point is indicated

Table 3 Performance of the training and test sets of the three-fold cross-validation

Fixed threshold	Percentage	Threshold	Test set	
			Sens	PPV
Training 1 (PPV: 0.92)	0.06	0.6050	0.92	1
Training 2 (PPV: 0.89)	0.20	0.4200	1	0.8929
Training 3 (PPV: 0.91)	0.30	0.3850	1	0.7931
Overall	–	–		
Variable threshold	**Percentage**	**Standard deviation**	**Test set**	
			Sens	PPV
Training 1 (PPV: 0.92)	0.06	5.4	1	1
Training 2 (PPV: 1.00)	0.06	5.4	1	0.8621
Training 3 (PPV: 0.93)	0.06	5.6	1	1
Overall	0.06	5.5		

The parameters used in the test set are obtained from the combination in the training set with a sensitivity of 1 with the highest obtainable PPV, which is also indicated in this table

with a circle on the ROC-curve shown in (a). The matching parameter combinations of this point are shown in Fig. 5b as white pixels. Each point in this figure represents a combination of a certain threshold (y-axis) and a percentage of vectors (x-axis). Notice that multiple combinations of the parameters yield optimal performance. The combination with the lowest values is situated in the left upper corner. The parameter combination used in the test set is indicated with a circle in this figure, and the values can be found in Table 3.

3.2.2 Second approach: variable threshold

The evaluation of this approach is similar to the first approach, but the threshold values in Fig. 5 are replaced by standard deviations. For each training set, multiple points are obtained with a sensitivity of one with a maximal PPV. Furthermore, multiple of these parameter combinations are the same in the three training sets, so the highlighted points in Fig. 5 overlap. As shown in Table 3 the best values for each training set are nearly the same. They give good results as in two test sets a sensitivity and PPV of 1 is reached and in the other test set a PPV of still 0.8621 is reached (when the sensitivity is one). The false positives here are caused by a flickering computer screen and a glitch in the video.

4 Discussion

The goal was to develop a detection algorithm based on video recordings to discriminate between movement and non-movement in nocturnal recordings from patients with epilepsy. We found that the usage of a variable threshold leads to better results in comparison to a fixed threshold, as the sensitivity in the three test sets when using the variable threshold was 1, with a corresponding PPV of 1, 0.8621, and 1. Furthermore, there was an overlap in the optimal points in the three test sets, which indicates that this value is robust for different datasets.

In Fig. 5b and also a bit in 5c, d, a linear trend is visible. This can be explained as follows. When the percentage of the highest motion vectors increases (more vectors are taken into account) the resulting signal $R(t)$ decreases as more vectors with a lower amplitude are taken. This will lower the optimal threshold and results in the correlation visible in Fig. 5b–d.

A different camera set-up may result in a different ideal fixed threshold. The variable threshold overcomes this problem. It will contain less false positives because the threshold is more adapted to the noise. A way to anticipate to changing environmental parameters during the acquisition (e.g. sunrise, which may influence the noise level) when using the algorithm in a real setting, an epoch without movement can be taken each hour and the threshold can be adapted accordingly. However, the approach with the variable threshold requires that the selected reference epoch is a good representation of the non-movement epochs in the sequence.

For a further reduction of the false positives we could integrate additional intelligence such as a human body detector, and only inspect $R(t)$ in this region. This would eliminate the false positive due to the flickering screen.

A system to detect movement events from epileptic patients was also studied in [16]. In this study three-dimensional accelerometers were used. The algorithm which was developed detected 100% of the movement epochs with a PPV between 43% and 89%, on a total dataset of 35 min of seven patients. Our algorithm gives a higher PPV. However, it should be noticed that some very subtle motions which occur under the blankets may not have been noticed by the expert in the video data, and hence accelerometer data can be useful in addition to the video data. A combination of both detection methods may result in a system with a sensitivity of one and a higher PPV than the one reached in each system separately for the detection of epileptic seizures.

A real-time implementation of the optical flow algorithm is necessary in the future, for example when an alarm has to be generated when a severe epileptic seizure occurs. Rowekamp and Peters [17] already implemented the Horn–Schunck optical flow algorithm in hardware. Their implementation reached a throughput of 50 frames per second for images with a resolution of 128 × 128. Chase et al. [3] compared a tensor-based implementation of the optical flow on an FPGA with the implementation using a GPU.

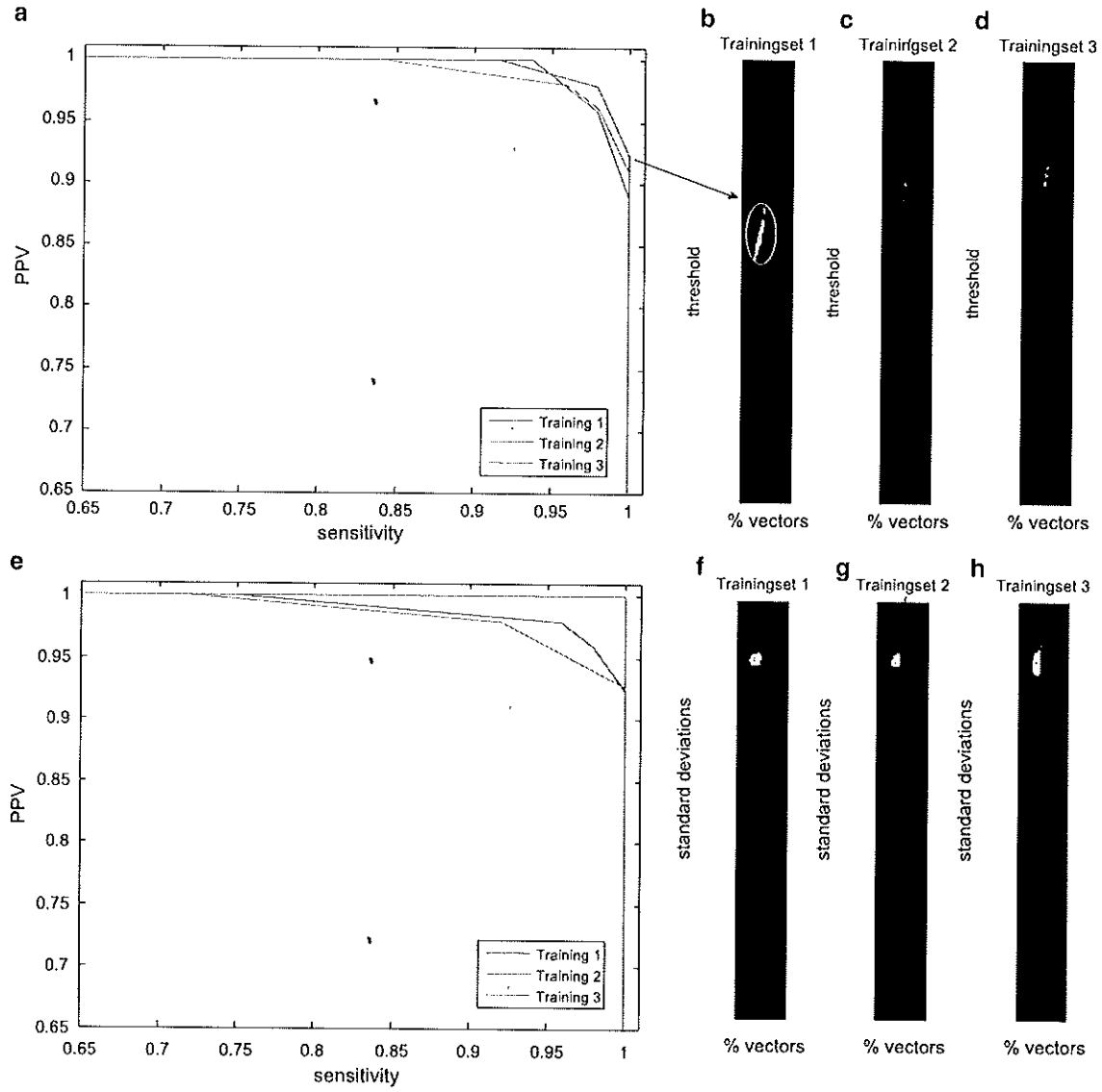


Fig. 5 Evaluation of three training sets for the fixed (**a–d**) and variable (**e–h**) threshold. **a** and **e** show the envelope for the ROC-curves for the different training sets. Notice that the *x*- and *y*-axis are zoomed in for a better visualization. For each optimal point in the ROC-curve (a sensitivity of one and the highest possible PPV) multiple parameter combinations are possible. The optimal point in the first training set indicated by a *circular mark* in (**a**) corresponds to the white pixels in (**b**). The parameter combinations used in the test set are marked with a *circle* in **b–d** and **f–h**

On the Yosemite sequence with a resolution of 640 × 480, both implementations had a similar performance of about 300 frames per second.

In this paper, we have made use of one aspect of the optical flow field, namely the extraction of the movement intensity $R(t)$. However, much more information can be extracted, such as different spatio-temporal patterns which could be characteristic for certain types of epileptic seizures. In this way the direction and intensity of the movement over time of different body parts can be taken into account. We see this approach as the next step in the detection and classification of seizures based on video data from the preselected dataset generated by the algorithm discussed in this paper.

Our future goal is to detect different kinds of epileptic seizures (pathological movement) in a home setting with only the video monitoring system. The algorithm developed in this paper, however, can also be used for the detection of movement of patients with sleeping disorders to measure the movement during the night and thus estimate the time the patient is awake. Also, an additional channel only based on the video recordings during video/EEG acquisitions at night could be beneficial in the further analysis of video-EEG data and treatment of patients with epilepsy.

The main message of this paper can be summarized by saying that nocturnal movement detection in epileptic pediatric patients using the optical flow algorithm is possible and a variable threshold seems to give a considerable better result than a fixed threshold, resulting in a sensitivity of one in the test sets and a corresponding PPV between 0.8621 and 1.

Acknowledgments Research supported by Research Council KUL: GOA-MANET, IWT: TBM070713-Accelero, Belgian Federal Science Policy Office IUAP P6/04 (DYSCO, 'Dynamical systems, control and optimization, 2007–2011); EU: Neuromath (COST-BM0601). Kris Cuppens' research funded by a Ph.D grant of the Institute for the Promotion of Innovation through Science and Technology in Flanders (IWT-Vlaanderen)

References

1. Bonroy B, Schiepers P, Leysens G, Miljkovic D, Wils M, De Maesschalck L, Quanten S, Triau E, Exadaktylos V, Berckmans D, Vanrumste B (2009) Acquiring a dataset of labeled video images showing discomfort in demented elderly. Telemed J E-Health 15(4):370–378
2. Bradski G, Kaehler A (2008) Learning OpenCV. O'Reilly Media
3. Chase J, Nelson B, Bodily J, Wei Z, Lee DJ (2008) Real-time optical flow calculations on FPGA and GPU architectures: a comparison study. In: FCCM '08: proceedings of the 2008 16th international symposium on field-programmable custom computing machines, IEEE Computer Society, Washington, DC, USA, pp 173–182
4. Conradsen I, Beniczky S, Wolf P, Terney D, Sams T, Sorensen HBD (2009) Multi-modal intelligent seizure acquisition (misa)? A new approach towards seizure detection based on full body motion measures. In: Proceedings of the 31st annual international conference of the IEEE EMBS, Minneapolis, Minnesota, USA, pp 2591–2595
5. Cuppens K, Lagae L, Vanrumste B (2008) Towards automatic detection of movement during sleep in pediatric patients with epilepsy by means of video recordings and the optical flow algorithm. In: Vander Sloten J, Verdonk P, Nyssen M, Haueisen J (eds) Proceedings of the 4th European congress of the international federation for medical and biological engineering (MBEC 2008), ECIFBME 2008, Antwerp, Belgium, IFMBE Proceedings, vol 22, pp 784–789
6. Cuppens K, Lagae L, Ceulemans B, Van Huffel S, Vanrumste B (2009) Detection of nocturnal frontal lobe seizures in pediatric patients by means of accelerometers: a first study. In: Proceedings of the 31st annual international conference of the IEEE EMBS, Minneapolis, Minnesota, USA, pp 6608–6611
7. Horn BKP, Schunck BG (1981) Determining optical-flow. Artif Intell 17(1–3):185–203
8. Hu WM, Tan TN, Wang L, Maybank S (2004) A survey on visual surveillance of object motion and behaviors. IEEE Trans Syst Man Cybern C 34(3):334–352
9. Jallon P, Bonnet S, Antonakios M, Guillemaud R (2009) Detection system of motor epileptic seizures through motion analysis with 3D accelerometers. In: Proceedings of the 31st annual international conference of the IEEE EMBS, Minneapolis, Minnesota, USA, pp 2466–2469
10. Karayiannis NB, Tao GZ, Frost JD, Wise MS, Hrachovy RA, Mizrahi EM (2006) Automated detection of videotaped neonatal seizures based on motion segmentation methods. Clin Neurophysiol 117(7):1585–1594
11. Kearney J, Thompson W (1988) Bounding constraint propagation for optical flow estimation. In: Aggarwal J, Martin W (eds) Motion understanding: robot and human vision. Kluwer Academic Publishers, Boston
12. Kim YH, Kak AC (2006) Error analysis of robust optical flow estimation by least median of squares methods for the varying illumination model. IEEE Trans Pattern Anal Mach Intell 28(9):1418–1435
13. Ko T (2008) A survey on behavior analysis in video surveillance for homeland security applications. 2008 37th IEEE Applied Imagery Pattern Recognition Workshop pp 84–91, 37th Applied Imagery and Pattern Recognition Workshop OCT 15–17, 2008 Washington, DC
14. Liu Q, Sclabassi RJ, Sun M (2004) Change detection in epilepsy monitoring video based on markov random field theory. In: Intelligent signal processing and communication systems, 2004. ISPACS 2004
15. Lucas BD, Kanade T (1981) An iterative image registration technique with an application to stereo vision. In: DARPA imaging understanding workshop, pp 121–130
16. Nijsen TME, Cluitmans PJM, Arends J, Griep PAM (2007) Detection of subtle nocturnal motor activity from 3-D accelerometry recordings in epilepsy patients. IEEE Transactions on Biomedical Engineering 54(11):2073–2081
17. Rowekamp T, Peters L (1997) A real-time smart sensor system for visual motion estimation. In: EDTC '97: proceedings of the 1997 European conference on design and test, IEEE Computer Society, Washington, DC, USA, p 613
18. Schepers HM, Roetenberg D, Veltink PH (2010) Ambulatory human motion tracking by fusion of inertial and magnetic sensing with adaptive actuation. Med Biol Eng Comput 48(1):27–37
19. Sonka M, Hlavac V, Boyle R (2008) Motion analysis. In: Image processing, analysis, and machine vision. Kluwer Academic Publishers, Dordrecht
20. Suzuki S, Matsui T, Kawahara H, Ichiki H, Shimizu J, Kondo Y, Gotoh S, Yura H, Takase B, Ishihara M (2009) A non-contact vital sign monitoring system for ambulances using dual-frequency microwave radars. Med Biol Eng Comput 47(1):101–105
21. Turaga P, Chellappa R, Subrahmanian VS, Udrea O (2008) Machine recognition of human activities: a survey. IEEE Trans Circuits Syst Video Technol 18(11):1473–1488
22. Wang LA, Hu WM, Tan TN (2003) Recent developments in human motion analysis. Pattern Recognit 36(3):585–601